Journal of Materials Processing Technology 209 (2009) 4802–4808

Contents lists available at ScienceDirect

Journal of Materials Processing Technology

journal homepage: www.elsevier.com/locate/jmatprotec

Precision machining of microstructures on electroless-plated NiP surface for molding glass components

Jiwang Yan*, Takashi Oowada, Tianfeng Zhou, Tsunemoto Kuriyagawa

Department of Nanomechanics, Graduate School of Engineering, Tohoku University, Aoba 6-6-01, Aramaki, Aoba-ku, Sendai 980-8579, Japan

ARTICLE INFO

Article history:
Received 29 October 2008
Received in revised form 13 December 2008
Accepted 20 December 2008

Keywords:
Micro-machining
Microstructure array
Glass molding
Optical components

ABSTRACT

Micro-cutting experiments were conducted on electroless-plated nickel phosphorous (NiP) surfaces to fabricate microstructures such as microgrooves and micropyramid arrays. Burr formation behavior and cutting force characteristics were investigated experimentally and simulated by the finite element method (FEM) under various conditions. A simple two-step cutting process was proposed to improve the surface quality. The machined microstructure arrays were used as molds for hot-press glass molding experiments and good geometrical transferability was confirmed. The results from this study verify that diamond-machined NiP microstructure molds are applicable to glass molding processes for mass production of precision micro-mechanical and optical components.

1. Introduction

Three-dimensional micro-surface structures such as arrays of microgrooves, micropyramids, microneedles, microlenses and microprisms are required more and more in recent optical, optoelectronic, mechanical and biomedical industries. Components with micro-surface structures yield new functions for light operation, thus improve significantly the imaging quality of optical systems (Yan, 2006). The microstructures can also be used as fluid channels in biomedical and biochemical applications. Therefore, high-precision and high-efficiency fabrication of the microstructures on flat or curved surfaces are receiving focused interests.

Glass and plastic are two major substrate materials for the micro-structured components. Glass has predominant advantages over plastic on aspects of hardness, refractive index, light permeability, stability to environmental changes in terms of temperature and humidity, and so on. A few microstructures on glass can be fabricated by material removal processes such as sand blasting, photolithography and wet/dry etching. These processes are effective for manufacturing microstructures with rectangular cross-sections, but difficult to fabricate microstructures with angled or curved cross-sections. Moreover, it is still difficult for these machining techniques to achieve optical-quality surfaces and precise structures with sharp edge profiles. Micro-cutting of glass with micro-end mills has also been reported, but the production efficiency is limited and the production cost is considerably high for mass production.

As an alternative approach, glass molding is a promising method to produce precision optical elements such as aspherical lenses, Fresnel lenses, diffractive optical elements (DOEs), microlens arrays, and so on (Katsuki, 2006; Masuda et al., 2007). In glass molding, the fabrication of the molding die is an important issue. Although hard materials such as silicon carbide (SiC), tungsten carbide (WC) and fused silica (SiO_2) are preferable mold materials for continuous surfaces, they have not been commonly used for molding microstructures because it is very difficult to generate microstructures on these materials.

Nickel–phosphorous (NiP) electroless plating has been known as an important mold surface preparation technology for manufacturing plastic optical parts. NiP plating provides hard, wear resistant and corrosion resistant surfaces at relatively high temperatures, and at the same time, maintains excellent precision micro-machinability (Yan et al., 2004). In a previous work (Masuda et al., 2007), the present authors have preliminary demonstrated that NiP plating can also be used for molding glass components, such as aspherical and diffractive lenses, with a considerably long mold service life. In the present study, the authors attempted to fabricate three-dimensional microstructures on the electroless-plated NiP mold surfaces by ultraprecision micro-cutting technology, and examined the geometrical transferability of the machined microstructures to glass during the hot-pressing process.

* *Corresponding author*. Tel.: +81 22 795 6946; fax: +81 22 795 7027.
E-mail address: yanjw@pm.mech.tohoku.ac.jp (J. Yan).

0924-0136/$ – see front matter © 2009 Elsevier B.V. All rights reserved.
doi:10.1016/j.jmatprotec.2008.12.008

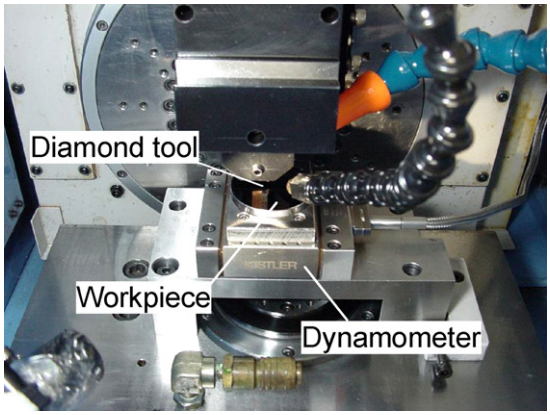

Fig. 1. Photograph of the micro-cutting setup.

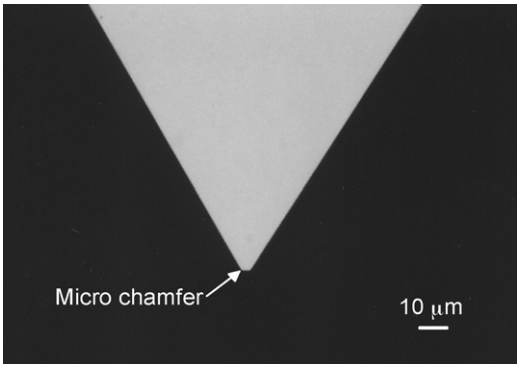

Fig. 2. SEM photograph of the micro-cutting tool with a micro-chamfered tip.

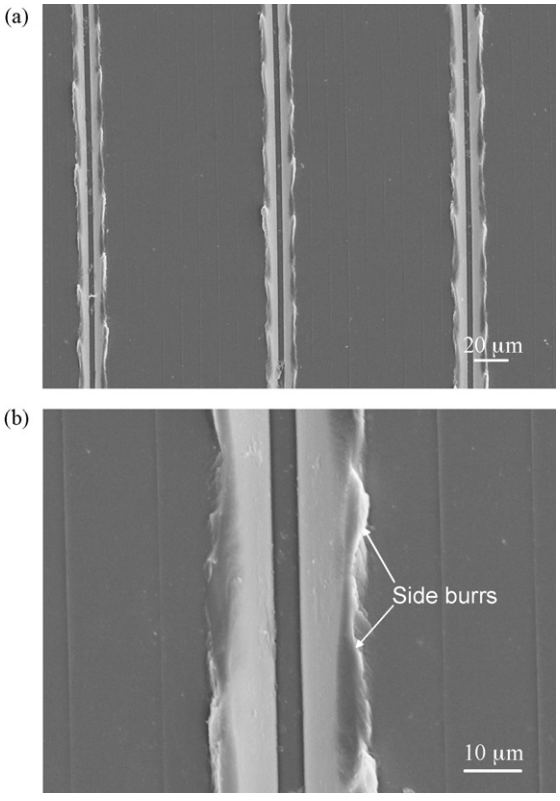

Fig. 3. SEM photographs at different magnifications showing microgrooves with side burrs.

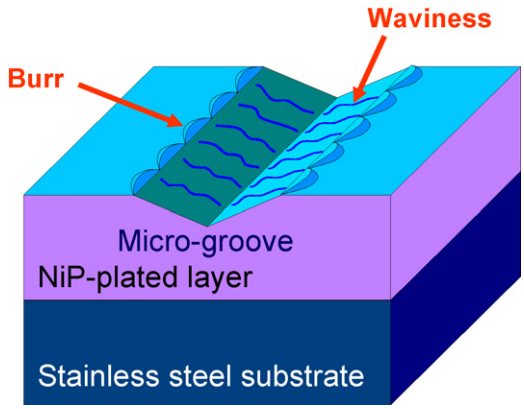

Fig. 4. Schematic presentation of side burrs and waviness formation in microgrooving process.

2. Experimental

2.1. Micro-cutting tests

Two kinds of microstructures were fabricated by micro-cutting: one is a microgroove array and the other is a micropyramid array. To cut microgrooves, a sharp diamond cutting tool is transversely fed in the horizontal direction while the depth of cut is kept constant. By periodically shifting the tool perpendicularly to the cutting direction, parallel microgroove arrays can be generated. After the groove arrays have been fabricated, the workpiece is then rotated for an angle of 90° on the horizontal plane, and the cross-grooving operation is performed under the same conditions. In this way, micropyramid arrays can be fabricated on the workpiece surface. Micro-cutting tests were done using an ultraprecision machine Toyoda AHN-05, produced by JTEKT Corporation, Japan. The machine enables its tables to move under four-axis (XYZB) numerical control at a stepping resolution of 1 nm. Fig. 1 is a photograph of the main section of the machine. A piezoelectric dynamometer, Kistler

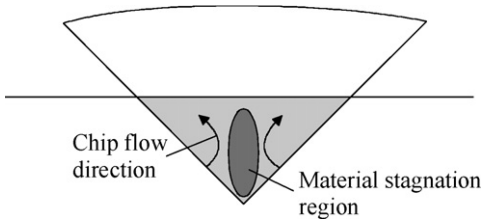

Fig. 5. Cross-sectional model for the one-step grooving process showing a material stagnation region.

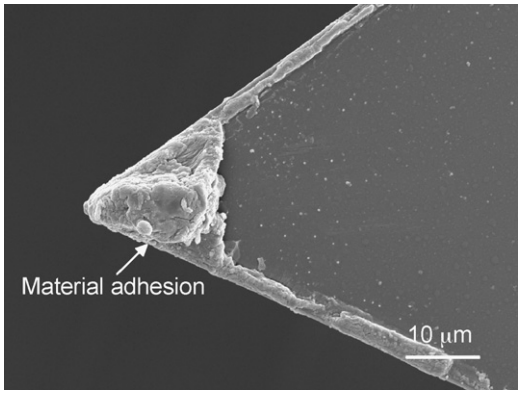

Fig. 6. SEM photograph of the tool tip showing material adhesion.

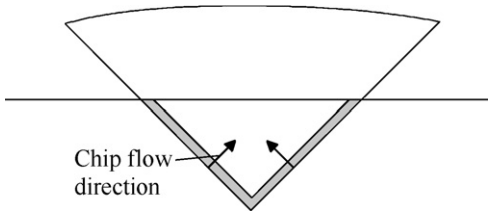

Fig. 7. Cross-sectional model of the second cut of the two-step microgrooving process.

9256A, was mounted below the workpiece to measure the micro-cutting forces during the cutting tests.

Two kinds of cutting tools made of single-crystal diamond were used: one is extremely sharpened tools with no width at the end, and the other has a 5 μm flat chamfer at the tool tip. Two kinds of tool included angles were used, namely 90° and 60°, respectively. The rake angle is 0° and the relief angle is 10° for all the tools. Fig. 2 is an SEM photograph of the tip of a micro-chamfered 60° diamond tool. A round stainless steel plate with a diameter of 50 mm, electroless-plated with NiP under specially controlled conditions, is applied as a test workpiece. Face turning was performed to flatten the NiP plated surface before machining microstructures. The depth and the pitch of the microgrooves were both changed from 1 μm to 20 μm. The cutting speed was set to 500 mm/min (0.0083 m/s). As lubricant Bluebe #LB10 cutting oil was used in form of a mist jet.

2.2. Glass molding tests

Glass molding experiments were conducted using an ultraprecision glass molding machine, GMP211, produced by Toshiba Machine Co. Ltd., Japan. A flat NiP-plated mold with machined microstructures and another flat NiP mold without microstructures were used as the lower mold and the upper mold, respectively. Nitrogen gas was used to purge the air to prevent the molds from oxidation at high temperatures. The molding chamber was covered by a trans-

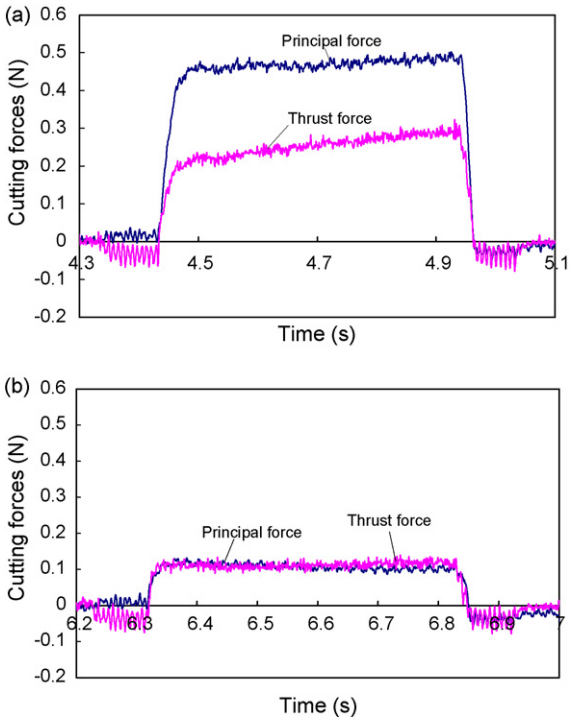

Fig. 8. Plots of cutting forces in microgrooving tests by the two-step cutting method: (a) the first cut and (b) the second cut.

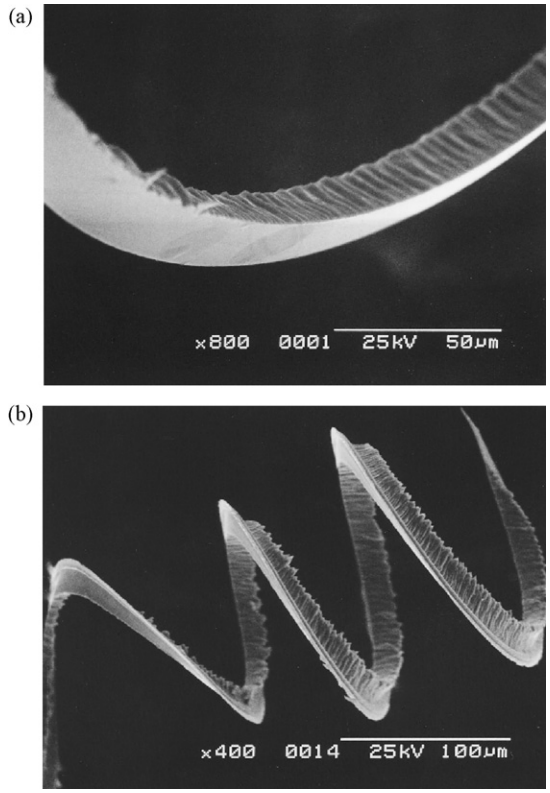

Fig. 9. SEM photographs of cutting chips in: (a) the first cut and (b) the second cut.

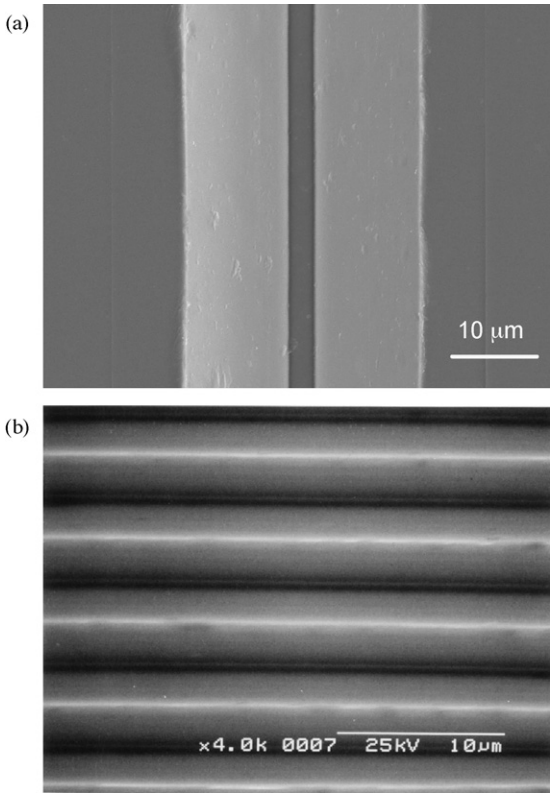

Fig. 10. SEM photographs of microgrooves obtained by two-step cutting method: (a) a single groove and (b) a groove array.

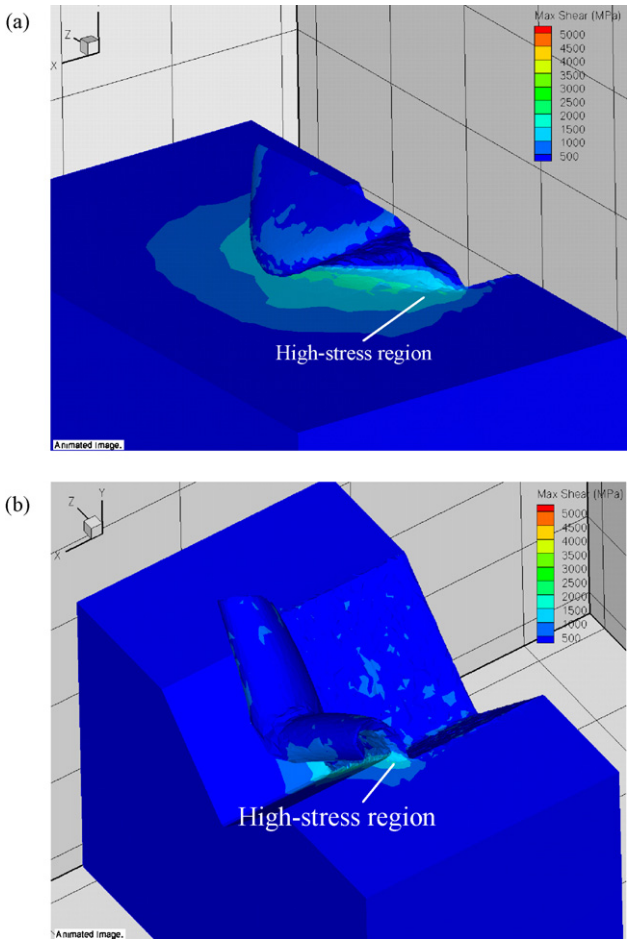

Fig. 11. FEM-simulated shear stress distributions in: (a) the first cut and (b) the second cut.

parent silica glass tube which can let the infrared rays in and separate the nitrogen gas from the air outside. Temperatures of the upper and lower molds are monitored by two thermocouples beneath their surfaces. During molding, the upper mold is remained stationary, and the lower mold is driven upward and downward by an AC servomotor. A load cell is placed beneath the lower axis as a feedback of the pressing load.

A commonly used glass, K-PG375, produced by Sumita Optical Glass, Inc., Japan, of cylindrical shape was used as test piece material. The transition point (T_g) of the glass is 343 °C, and the yielding point (A_t) is 363 °C, respectively. The molding temperature was set to 387 °C. At this temperature glass behaves as a viscous liquid and most of material deformation can be achieved at a low load (Yan et al., 2008). A low pressing load is essential in molding microstructures to protect the fine mold profiles from damages and deformation.

3. Results and discussion

3.1. Microgrooving tests

Burr formation was found to be a critical problem in microgrooving processes, especially in dry cutting or when the cutting fluid is not sufficiently provided into the cutting region (Yan et al., 2004). Fig. 3 shows scanning electron microscope (SEM) photographs (taken at different magnifications) of microgrooves cut by single cuts at a depth of 10 μm with a micro-chamfered 60° tool. It can be seen that burr formation at the side edges of the microgroove is very significant, although the inner surface of the groove is smooth. Within a few microgrooves surface waviness perpendicular to the grooving direction was also observed at the groove bottom. Fig. 4 shows schematically the formation model of side burrs and waviness in the microgrooving process.

The burr formation is presumably caused by the side flow of material in the cutting region. As shown in Fig. 5, the cross-section of the uncut chip is triangular, which is distinctly different from normal orthogonal cutting conditions where uncut chip thickness is uniform along the cutting edge. Therefore, during cutting, material flows generated by the two side edges are directed towards the center of the tool and interfere with each other, leading to a high-pressure material stagnation zone. The material stagnation at the tool center will cause significant side flows of material to form side burrs. At the same time, microscopic waviness may occur due to the unsteadiness of material flow and fluctuation of cutting forces. This problem is especially serious when cutting deep grooves or grooves with high aspect ratios.

To examine the occurrence of material stagnation, SEM observation of the tool tip was performed after cutting. Fig. 6 is an SEM photograph of the tool tip where material adhesion can be seen. Material stagnation causes a highly negative effective tool rake angle, and in turn, increases the cutting forces. The phenomenon of material stagnation can be partially prevented by applying cutting fluid effectively into the cutting region, but it is difficult to completely eliminate it. To eliminate burr formation in microgrooving, Kim et al. recently attempted ultrasonic vibration-assisted cutting (Kim and Loh, 2007). Vibration can prevent from material stagna-

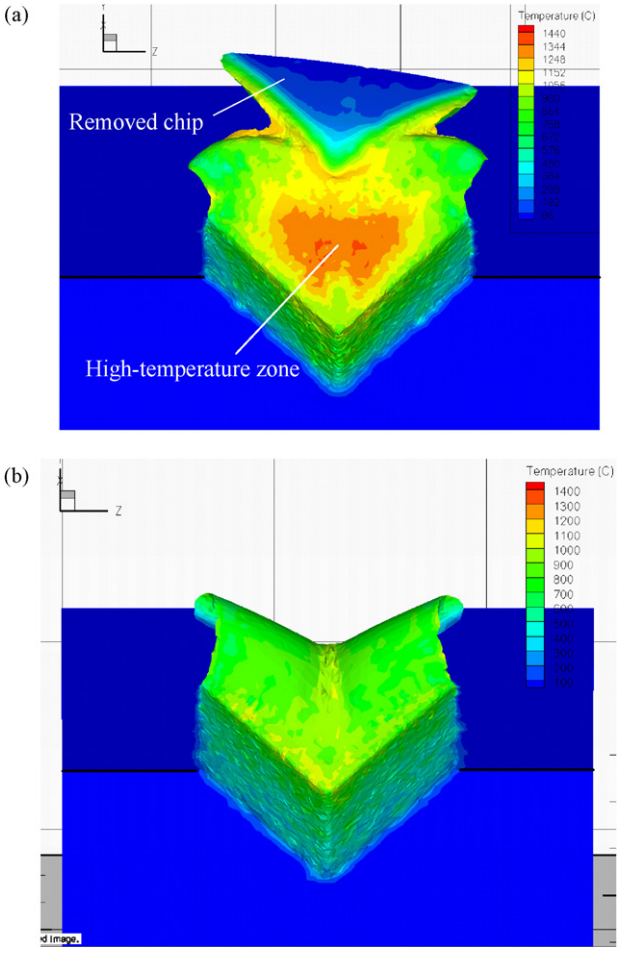

Fig. 12. FEM-simulated temperature distributions in: (a) the first cut and (b) the second cut.

tion, thus is helpful for eliminating burr formation, but meanwhile, increases the surface roughness of the inner groove surfaces.

As one of the solutions to the burr-formation problem, the authors simply performed two-step cutting experiments. That is, the first cut is done as a rough cut at a large depth, and the second cut is done as a finish cut at a small chip thickness (~1 μm). In this case, the cutting model of the finish cut is shown schematically in Fig. 7. The cutting conditions at both side edges are similar to the orthogonal cutting state. This way, the material flow will be fluent and steady, which contributes to burr-free surface formation.

Fig. 8 is a comparison of the cutting force characteristics. It can be seen that in the first cut (depth of cut 9 μm) of the two-step cutting, the principal force is remarkably higher than the thrust force. However, in the second cut (depth of cut 1 μm), the principal force and the thrust force are at the same level, indicating that a burnishing effect is obtained. In addition, force amplitudes and force fluctuations in Fig. 8(b) are both smaller than those in Fig. 8(a). Fig. 9 is a comparison of chip geometry. In the first cut of the two-step cutting, triangular cross-section chip is formed; whereas in the second cut, the chip has a V-shaped cross-section with a uniform thickness. Fig. 10 shows SEM photographs of a single microgroove and groove arrays obtained using the two-step cutting method. The groove surfaces are extremely smooth and no burrs can be seen. Currently it has not been possible to measure the roughness and waviness of the inclined surfaces within the microgrooves. Further work is continuing to characterize these aspects.

3.2. FEM simulation of cutting temperature and stress

In order to investigate the stress and temperature distribution in the microgrooving process, finite element method (FEM) simulation was done using the commercially available software AdvantEdge produced by Third Wave Systems, Inc., USA. Due to the fact that NiP was not available as a workpiece material within the menu of AdvantEdge, a Ni-based alloy M35P was chosen, judged to be close to NiP in material properties. As a result, the simulation results in this paper must be considered as for guidance only.

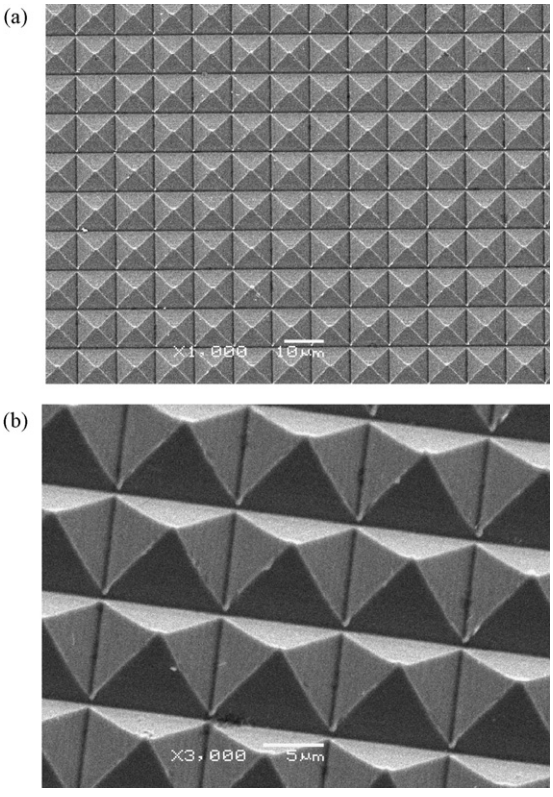

Fig. 13. SEM photographs of micropyramids array fabricated by the cross-grooving method: (a) front view and (b) inclined view.

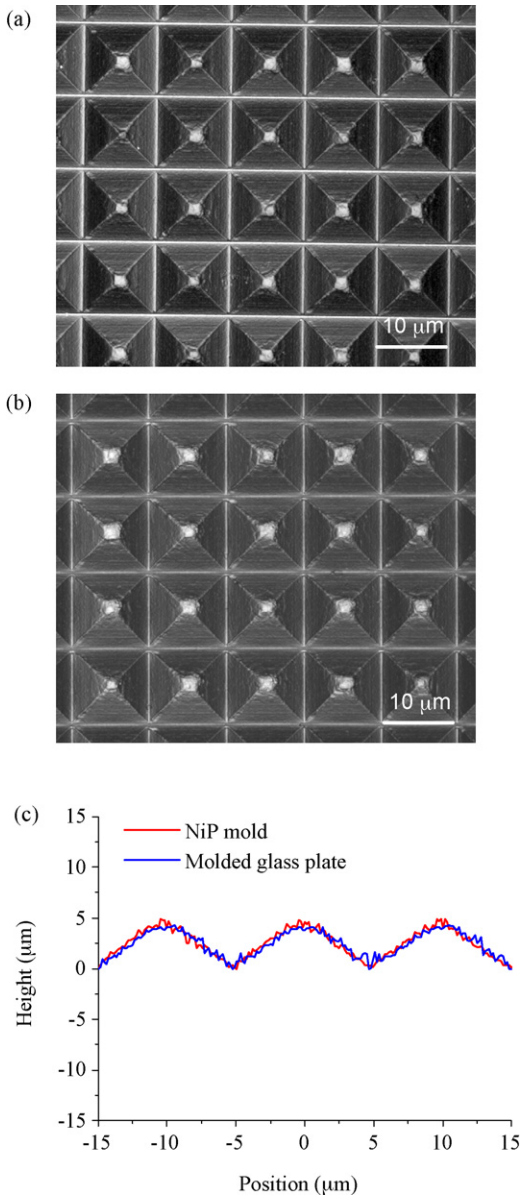

Fig. 14. Microscope images of micropyramid arrays on: (a) NiP mold and (b) molded glass plate; (c) is a comparison of the cross-sectional profiles of the NiP mold and the molded glass.

Fig. 11(a) and (b) shows distributions of shear stress in the cutting region during the first cut and second cut, respectively, of the two-step cutting process. In Fig. 11(a), the chip cross-section is triangular and a high-stress region is extending to a very broad area around the cutting tool, indicating a severe material deformation. In Fig. 11(b), however, the chip is very thin and uniform. The high-stress region is limited to the region just near the cutting edge. Since the volume of the plastically deformed material near the side cutting edge is directly related to the size of side burrs, the simulation results in Fig. 11 indicate that the burr formation in the second cut will be remarkably smaller than that in the first cut.

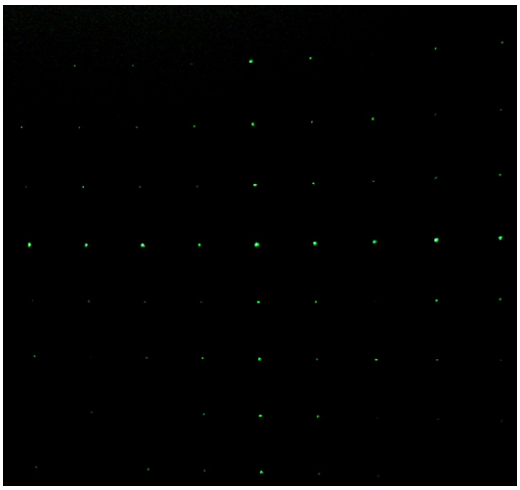

Fig. 15. Projection pattern obtained by directing a green laser beam perpendicularly to the glass surface structured with micropyramids. (For interpretation of the references to color in this figure legend, the reader is referred to the web version of the article.)

Fig. 12 shows FEM-simulated distributions of cutting temperature in the workpiece material contacting with the tool rake face. It should be pointed out that the simulated temperature values in this figure may not be quantitatively accurate and are only used for qualitative comparison. In Fig. 12(a), a high temperature region can be clearly seen in the center of the chip. This high-temperature region may cause softening, melting and adhesion of workpiece material (see Fig. 6), which contributes to burr formation. However, in Fig. 12(b), the temperature is remarkably lower than that in Fig. 12(a), and the temperature distribution is uniform. The simulation results of temperature demonstrate again that a small undeformed chip thickness in the microgrooving process is important for preventing burr formation.

3.3. Glass molding tests of microstructures

Fig. 13 shows front view and inclined view SEM photographs of micropyramid arrays fabricated on the NiP surface with a 90° diamond tool. The height and the width of the pyramids are 5 μm and 10 μm, respectively. Cutting was performed by the two-step cutting method where the first cut was done at a depth of 4 μm and the second cut was performed at a depth of 1 μm. In Fig. 13(b), extremely small burrs hardly resolvable can be seen at the downward-facing left side edges of the micropyramids. However, they are so small as to have little effect on the optical functions of the molded surface.

Finally, the microstructured NiP surfaces were used as molding dies for glass molding tests. Fig. 14(a) and (b) is microscope images of micropyramid arrays on the NiP mold surface and the pyramid arrays molded onto the glass surface, respectively. Fig. 14(c) is a comparison of the cross-sectional profiles of the NiP mold and the molded glass plate measured by a laser microscope VK-8500, produced by Keyence Corporation. From Fig. 14, it is evident that the shape of the micropyramids on the NiP surface has been precisely transcribed to the glass surface. The surface of glass pyramids is as smooth as that of the NiP mold. These kinds of micropyramids may be used as new optical elements (Lee et al., 2006; Lin et al., 1998). For example, Fig. 15 shows the projection pattern obtained on a screen when a green laser beam (wavelength 532 nm) was directed perpendicularly to the glass plate surface structured with micropyramids as shown in Fig. 14. Due to the interference between the laser beams split by the side faces of the micropyramid, numerous regularly arranged laser spots are clearly formed on the screen.

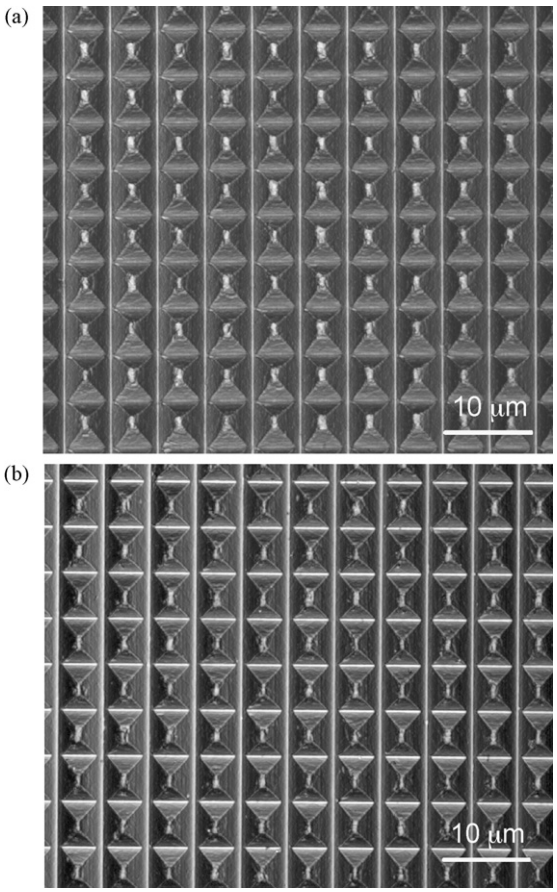

Fig. 16. Microscope images of micro-channel arrays on: (a) NiP mold and (b) molded glass plate.

Fig. 16 is another example of glass molding tests. The micro-channel array in Fig. 16(a) is obtained on NiP surface by cross-grooving at different depths between the horizontal cuts and the perpendicular cuts. After molding, the micro-channels on glass in Fig. 16(b) look identical to those on the NiP mold in Fig. 16(a). After molding micropyramid arrays for 50 shots, the NiP mold was taken out of the molding machine and observed using a microscope. No obvious damage and deformation of the mold was seen. Although the mold service life tests have not been performed in this paper, it is presumable that the mold can be used for nearly one thousand shots, similar to that in molding glass lenses (Masuda et al., 2007).

4. Conclusions

Main conclusions drawn from the present study can be summarized as follows.

(1) In one-step cutting of micro-V-grooves burrs occur at the groove edges due to the side flows of material. Material stagnation in front of the tool causes temperature rise, cutting force increase and chip adhesion to the tool.
(2) By introducing a finishing cut at a small undeformed chip thickness approaching the orthogonal cutting conditions, the burr formation can be eliminated effectively.
(3) Microgrooves and micropyramid arrays with a depth ranging from one-micron level to 10-micron level can be precisely generated by micro-cutting with sharpened single-crystalline diamond tools.

(4) Diamond-machined microstructures on electroless-plated NiP molds can be precisely transcribed to glass surfaces by repetitive hot-press molding, which provides a high-efficiency manufacturing method for micro-optical components of glass.

Acknowledgements

The authors would like to thank Third Wave Systems, Inc., for providing the cutting simulation software. This work has been supported by Japan Society for the Promotion of Science, Grant-in-Aid for Scientific Research (B), project number 19360055.

References

Katsuki, M., 2006. Transferability of glass lens molding. In: Proceedings of SPIE, 2nd International Symposium on Advanced Optical Manufacturing and Testing Technologies, Xi'an, China, p. 61490.

Kim, G.D., Loh, B.G., 2007. An ultrasonic elliptical vibration cutting device for micro V-groove machining: kinematical analysis and micro V-groove machining characteristics. Journal of Materials Processing Technology 190, 181–188.

Lee, J.Y., Kim, Y.J., Nahm, K.B., Ko, J.H., 2006. Optical simulation of micro-pyramid arrays for the applications in the field of backlight unit of LCD. In: IMID/IDMC '06 DIGEST, pp. 1343–1346.

Lin, L., Cheng, Y.T., Chiu, C.J., 1998. Comparative study of hot embossed micro structures fabricated by laboratory and commercial environments. Micro System Technologies 4, 113–116.

Masuda, J., Yan, J., Kuriyagawa, T., 2007. Application of the NiP-plated steel molds to glass lens molding. In: Proceedings of the 10th International Symposium on Advances in Abrasive Technology, Dearborn, USA, pp. 123–130.

Yan, J., Sasaki, T., Tamaki, J., Kubo, A., Sugino, T., 2004. Chip formation behavior in ultra-precision cutting of electroless nickel plated mold substrates. Key Engineering Materials 3–8, 257–258.

Yan, J., 2006. Ultraprecision machining for Fresnel lenses and their molds. In: Design and Manufacturing of Rear-Projection Optical Systems. Technical Information Institute, Tokyo, pp. 73–94.

Yan, J., Zhou, T., Masuda, J., Kuriyagawa T., 2008. Modeling high-temperature glass molding process by coupling heat transfer and viscous deformation analysis. Precision Engineering, doi:10.1016/j.precisioneng.2008.05.005.